

ANALYTIC SOLUTION FOR SELF-REGULATED COLLECTIVE ESCAPE OF COSMIC RAYS FROM THEIR ACCELERATION SITES

M. A. MALKOV^{1,2}, P. H. DIAMOND^{1,7}, R. Z. SAGDEEV³, F. A. AHARONIAN^{4,5}, AND I. V. MOSKALENKO⁶

¹ CASS and Department of Physics, University of California, San Diego, La Jolla, CA 92093, USA; mmalkov@ucsd.edu, pdiamond@ucsd.edu

² Kavli Institute for Particle Astrophysics and Cosmology, Stanford, CA 94305, USA

³ University of Maryland, College Park, MD 20742-3280, USA

⁴ Dublin Institute for Advanced Studies, 31 Fitzwilliam Place, Dublin 2, Ireland

⁵ Max-Planck-Institut für Kernphysik, P.O. Box 103980, D-69029 Heidelberg, Germany

⁶ Hansen Experimental Physics Laboratory, Stanford University, Stanford, CA 94305, USA

Received 2012 December 14; accepted 2013 March 18; published 2013 April 16

ABSTRACT

Supernova remnants (SNRs), as the major contributors to the galactic cosmic rays (CRs), are believed to maintain an average CR spectrum by diffusive shock acceleration regardless of the way they release CRs into the interstellar medium (ISM). However, the interaction of the CRs with *nearby* gas clouds crucially depends on the release mechanism. We call into question two aspects of a popular paradigm of the CR injection into the ISM, according to which they *passively* and *isotropically* diffuse in the prescribed magnetic fluctuations as test particles. First, we treat the escaping CR and the Alfvén waves excited by them on an equal footing. Second, we adopt field-aligned CR escape outside the source, where the waves become weak. An exact analytic self-similar solution for a CR “cloud” released by a dimmed accelerator strongly deviates from the test-particle result. The normalized CR partial pressure may be approximated as $\mathcal{P}(p, z, t) = 2[|z|^{5/3} + z_{\text{dif}}^{5/3}(p, t)]^{-3/5} \exp[-z^2/4D_{\text{ISM}}(p)t]$, where p is the momentum of CR particle, and z is directed along the field. The core of the cloud expands as $z_{\text{dif}} \propto \sqrt{D_{\text{NL}}(p)t}$ and decays in time as $\mathcal{P} \propto 2z_{\text{dif}}^{-1}(t)$. The diffusion coefficient D_{NL} is strongly suppressed compared to its background ISM value D_{ISM} : $D_{\text{NL}} \sim D_{\text{ISM}} \exp(-\Pi) \ll D_{\text{ISM}}$ for sufficiently high field-line-integrated CR partial pressure, Π . When $\Pi \gg 1$, the CRs drive Alfvén waves efficiently enough to build a *transport barrier* ($\mathcal{P} \approx 2/|z|$ —“pedestal”) that strongly reduces the leakage. The solution has a spectral break at $p = p_{\text{br}}$, where p_{br} satisfies the equation $D_{\text{NL}}(p_{\text{br}}) \simeq z^2/t$.

Key words: acceleration of particles – cosmic rays – diffusion – ISM: individual objects (W44, W51C, IC 443, W28) – ISM: supernova remnants

Online-only material: color figures

1. INTRODUCTION

The generation of cosmic rays (CRs) in supernova remnant (SNR) shocks by the diffusive shock acceleration (DSA) mechanism (e.g., Drury et al. 2001) is understood reasonably well up to the point of their escape into SNR surroundings. But making this mechanism responsible for the most of galactic CRs requires understanding all stages of the CR production including their escape from the accelerators. In fact, the best markers for “CR-proton factories” are nearby molecular clouds (MCs) illuminated by protons leaking from SNRs. CRs will be visible in gamma rays generated by collisions with protons in the cloud (Aharonian et al. 1994, 2008; Aharonian & Atoyan 1996; Gabici et al. 2009; Tavani et al. 2010; Abdo et al. 2010a, 2010b; Giuliani et al. 2011; Ellison & Bykov 2011; Torres et al. 2011). Whether this gamma radiation is detectable with current instruments depends on the CR leakage rate from the source. The recent surge in measurements of gamma-bright SNR suggests that the sensitivity threshold have already been surpassed for at least several galactic SNRs and it is becoming increasingly timely to improve our understanding of the CR leakage from these objects.

Without such improvement, it is also difficult to resolve the ongoing debates about the primary origin of gamma emission from some of the gamma-active remnants in complicated environs, e.g., RX J1713 (e.g., Funk 2012; Inoue et al. 2012;

Ackermann et al. 2013). In arguing for hadronic or leptonic origin, one needs to know exactly how far the CRs are spread from the source at a given time and with what spectrum. Indeed, strong self-confinement of accelerated CRs may keep their flux through a remote MC below the instrument threshold, primarily (and counterintuitively) for powerful accelerators. Conversely, self-confinement will enhance illumination of nearby MCs, thus enhancing the odds of detecting the hadronic contribution to the emission. Apart from the distance to the target MC, equally important is its magnetic connectivity with the CR source. Overall, the predictions for the emissivity of MCs near strong CR sources can differ from the test-particle (TP) results by an order of magnitude or more.

To better understand the physics of CR confinement to SNRs, we consider the CR escape separately from their acceleration, which is assumed to have faded because of the SNR age. Specifically, we will formulate the problem as a diffusion of a CR cloud (CRC) released from an accelerator into the interstellar medium (ISM) and propagating through a “gas” of self-excited Alfvén waves. At the scales larger than the initial size of the cloud, the solution, after an adjustment to the local environments, will become self-similar, depending only on the background diffusivity D_{ISM} and the integrated CRC energy (cf. the Sedov–Taylor (ST) solution for the point explosion).

The idea that the CRC confinement should be thought of as a *self-confinement* is not new (e.g., Wentzel 1974; Achterberg 1981). However, the analytic solution for CR propagation being uniformly valid in both the nearby and far zones of the initial

⁷ Also at WCI Center for Fusion Theory, NFRI, Korea.

CRC seems to be unknown. This paper is aimed at presenting and analyzing such a solution. With some reservations, it may also be applied to a late stage of CR acceleration in an SNR, when the accelerated CRs become disconnected from the shock and diffuse outward. Their pressure, however, is still sufficient to drive strong Alfvén waves that limit the CR escape. We begin with a brief discussion of the problems with the current escape models, thus motivating the new one.

1.1. The Need for a New CR Escape Model

Traditionally, the transport of CRs is treated differently inside and outside a DSA accelerator. Outside, CRs are thought to escape as TPs with a diffusion coefficient inferable from observations. This picture cannot be correct near the accelerator because the CR transport must be in a *self-confinement* regime, in which the CR streaming instability diminishes their diffusion coefficient by orders of magnitude. This CR anisotropy instability, and particularly its nonresonant extensions, macroscopically driven by the CR current and the CR pressure gradient, has a potential to generate magnetic field fluctuations well in excess of the ambient magnetic field, $\delta B \gtrsim B_0$ (e.g., Bell 2004; Drury & Falle 1986; Bykov et al. 2009; Malkov et al. 2010). At the very least, such strong fluctuations should justify the standard DSA assumption about the Bohm diffusion regime with the mean free path (mfp) of the order of the particle gyroradius, r_g , achieved at $\delta B \sim B_0$. Naturally, the transport is isotropic in this regime. The ISM background turbulence, on the other hand, is much weaker $\delta B^2/B_0^2 \lesssim 10^{-5}$ at the CR relevant length scales, thus resulting in the CR mfp $\gtrsim 10^5 r_g$ (for GeV particles, $r_g \gtrsim 10^{12}$ cm). It is important to emphasize that under these circumstances the cross-field diffusion coefficient, κ_{\perp} , is suppressed by a large factor compared to the diffusion along the field line, κ_{\parallel} , i.e., $\kappa_{\perp}/\kappa_{\parallel} \sim (\delta B/B_0)^4$ (see, e.g., Drury 1983).

It follows then that there is a problem of describing particle transport between the self-confinement (accelerator vicinity) and the TP (far from accelerator) transport regimes. To circumvent this problem, the acceleration process has been treated separately from the particle escape using one of two devices: the upper cutoff momentum and the free-escape boundary (FEB; see, e.g., Reville et al. 2009; Drury 2011, for recent discussions). As the names suggest, accelerated particles escape instantly upon reaching a prescribed boundary either in momentum or in configuration space. Their escape is assumed to have no effect on the acceleration other than through the modification of the shock structure (Moskalenko et al. 2007). In a simplified visualization of the DSA as a “box” process, suggested by Drury et al. (1999), the upper cutoff and the FEB are two sides of the box in the particle phase space. There were efforts to include self-generated waves into the description of particle acceleration and escape from strongly modified CR shocks (Malkov et al. 2002; Malkov & Diamond 2006), or in numerical treatments (Galinsky & Shevchenko 2007, 2011; Fujita et al. 2011). In most approaches, however, a sudden jump in the CR diffusion coefficient in momentum space is introduced to set an upper cutoff (e.g., Ptuskin & Zirakashvili 2005; Yan et al. 2012). A similar jump in coordinate space would result in an FEB.

As long as the CR transport outside the accelerator is treated in the TP approximation, no smooth transition between the CR acceleration and their escape is provided, regardless of the scenario for the latter. However, the diffusion coefficient rises by roughly five orders of magnitude in a transition zone that should be correspondingly large, unlike an infinitely thin FEB. It is this zone where the CR escape flux and confinement time

are set by self-generated waves, thus rendering the FEB a rather implausible concept. For many SNRs it is then not yet possible to conclude whether the gamma emission is leptonic or hadronic, should such a conclusion depend on the CR escape and on the subsequent illumination of adjacent clouds. In a broader sense, there is a missing link in galactic CR generation between the CR acceleration (under a very strong self-generated wave–particle scattering) and their subsequent propagation (in a very weak interstellar turbulence). The goal of this paper is to establish such a link.

Our treatment below is applicable to the following two situations. In one situation, a shock accelerates particles continuously but some of them reach far enough or diffuse across the local field to become disconnected from the shock front and have thus chances to escape. While doing so, they drive their own waves at a gyroradius scale, whose amplitudes gradually decrease outward and so does the particle density. The second situation is a clear-cut case for this paper that deals with a CRC released into the ISM with no ongoing acceleration inside the CRC. Both situations correspond to a mesoscale transport regime, intermediate between the Bohm diffusion inside the accelerator and a global, quasi-isotropic CR diffusion in the Galaxy. The latter process is, in turn, supported by a random large-scale component of the galactic magnetic field at the scale of tens of parsecs superposed on the regular, spiral-arm-aligned toroidal field (Brunetti & Codino 2000; Strong et al. 2007; Blasi & Amato 2012). In the mesoscale transport regime, however, these components are considered as an ambient field with a scale much larger than the CR gyroradius and even larger than the CRC scale height. Before we describe in the next section the physical setting of the problem, it is worthwhile to emphasize some of the qualitative results.

First of all, for sufficiently high initial CR pressure (higher than magnetic pressure) and low ambient turbulence level, $\delta B \ll B_0$, the spreading of the CRC strongly deviates from the oft-used TP solution. Instead of being controlled by only one (diffusive) scale $l_D \sim \sqrt{D_{\text{ISM}} t}$, the structure of the expanding CRC is more complicated. Namely, it comprises three zones, of which only the outermost has the above TP scaling, but a significantly *lower* CR pressure than it would maintain by diffusing through the ISM with the diffusivity D_{ISM} . Conversely, the CR pressure in the innermost part remains strongly enhanced. These two zones are connected by a self-similar, $1/z$ -part of the CR pressure profile.

2. CR ESCAPE MODEL

After the ST expansion stage in which the shock radius increases as $R_s \propto t^{2/5}$ and particularly in and after the so-called pressure-driven snowplow stage with a slower expansion at or below $R_s \propto t^{0.3}$ (e.g., Bisnovatyi-Kogan & Silich 1995; Truelove & McKee 1999), the diffusive propagation of CRs away from the shock becomes more important than their bulk expansion driven by the overpressured SNR interior. Regardless of the escape mechanism, one of the most important parameters is the number of spatial dimensions involved (see, e.g., Drury 2011 for a recent discussion). Indeed, the three-dimensional random walk is non-recurrent, so only the finite shock radius gives the particle a chance to return to it. However, two- and three-dimensional random walks are recurrent. Therefore, the first important assumption to make is, indeed, about the process dimensionality which immediately translates into the choice of magnetic field configuration. Note that since particles recede from the shock as $\bar{R} \propto t^{1/2}$, they escape already at the ST stage.

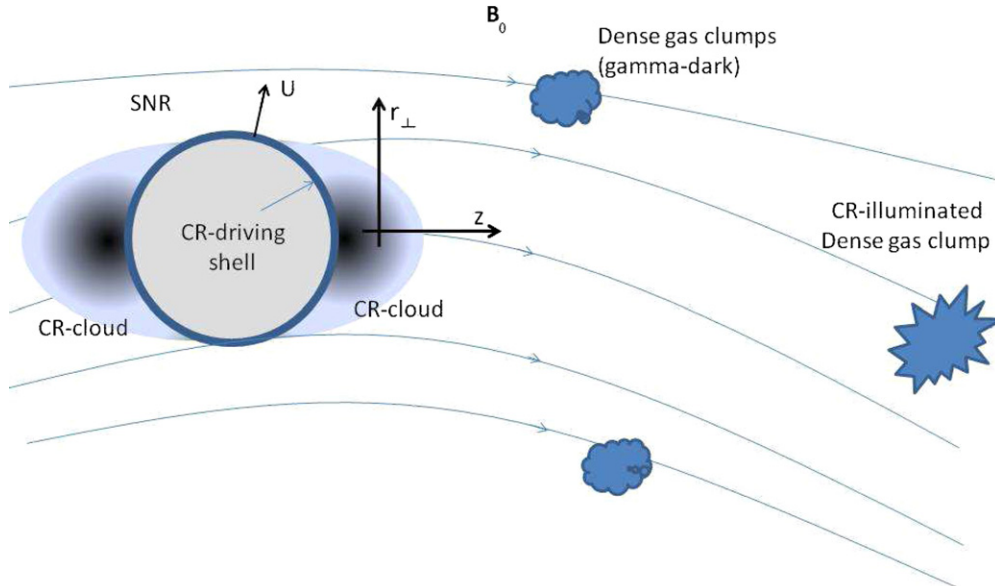


Figure 1. CR escape along the magnetic field \mathbf{B}_0 from the two polar cusps of SNR with a stalled blast wave. (A color version of this figure is available in the online journal.)

Contrary to the recent analytic (Drury 2011; Ohira et al. 2011; Yan et al. 2012) and numerical (with self-driven Alfvén waves; Fujita et al. 2011) treatments of the spherically symmetric particle escape, we consider an escape through the local flux tube. This choice is suitable for an SNR expansion in an ISM with a distinct large-scale magnetic field direction that does not change very strongly on the SNR scale. As we stated in the Introduction, our goal is to fill the gap between the weak scattering propagation far away from the remnant and the Bohm diffusion regime near the shock, with $\kappa = \kappa_B$. The perpendicular diffusion in the far zone is of the order of $\kappa_{\perp} \sim (\delta B/B_0)^2 \kappa_B \ll \kappa_B \ll \kappa_{\parallel} \sim (\delta B/B_0)^{-2} \kappa_B$, so we may safely assume that in the unperturbed ISM the diffusive propagation is one dimensional, along the field line.

Closer to and inside the accelerator (or rather in the region of its past activity), $\kappa_{\perp} \sim \kappa_{\parallel} \sim \kappa_B$, which favors the isotropy assumption. However, we may integrate (average) the equations for the CR transport and wave generation across the magnetic flux tube. Then, the problem becomes, again, formally one dimensional. However, the lateral expansion of the integrated flux tube may decrease CR pressure inside, thus making the CR self-confinement in the field direction less efficient. To estimate this effect we compare the “perpendicular” confinement time $\tau_{\perp} \sim a_{\perp}/U_{\perp}$ with the “parallel” confinement time $\tau_{\parallel} \sim a_{\parallel}^2/D_{\text{eff}}$. Here, $a_{\perp, \parallel}$ denote the respective sizes of the CRC, U_{\perp} is the expansion velocity across magnetic field, and D_{eff} is the effective CR diffusion coefficient along the field. We may estimate U_{\perp} from the balance of the CR pressure (assuming $P_{\text{CR}} \gg B^2/8\pi$) and the ram pressure of the ambient medium, $U_{\perp} \sim \sqrt{P_{\text{CR}}/\rho}$. The effective diffusivity, associated with the half-life of the CR against losses in the field direction, is shown in Appendix B to be $D_{\text{eff}} \sim \sqrt{D_{\text{ISM}} D_{\text{NL}}}$, where D_{NL} is the CR diffusivity suppressed by the self-generated Alfvén waves. Requiring $\tau_{\perp} \gg \tau_{\parallel}$ and estimating $a_{\perp} \sim R_{\text{SNR}}$, $a_{\parallel} \sim \kappa_B/U_{\text{sh}}$, we convert the inequality $\tau_{\perp} \gg \tau_{\parallel}$ into the following constraint on the CR acceleration efficiency $P_{\text{CR}}/\rho U_{\text{sh}}^2 < (U_{\text{sh}} R_{\text{SNR}}/\kappa_B)^2 (D_{\text{NL}} D_{\text{ISM}}/\kappa_B^2)$, where U_{sh} is the shock velocity. As both factors in the parentheses on the

right-hand side are larger than unity, the above requirement is fulfilled. The CRs then indeed escape along the field line before they inflate the flux tube significantly (cf., e.g., Rosner & Bodo 1996; Ptuskin et al. 2008, where the field-aligned propagation from CR sources has also been adopted). A schematic example of the basic configuration is shown in Figure 1. It should be noted that our simplified CR propagation scenario does not include possibly important perpendicular CR transport due to the CR drifts, magnetic field meandering, or turbulence spreading.

The second important assumption to make is about the spatial arrangement of the initial CR population. As shown in Figure 1, we adhere to the idea that the acceleration is most efficient in the quasi-parallel shock geometry. It can be advocated on the theoretical grounds (Malkov & Völk 1995; Völk et al. 2003), by in situ observations of heliospheric shocks, and hybrid simulations (e.g., Burgess et al. 2012; Gargaté & Spitkovsky 2012). More importantly, this acceleration preference is supported by SNR observations (e.g., Reynoso et al. 2013). Therefore, we may specifically assume that two “polar cusps” of accelerated particles are left behind after the acceleration has either faded out or entered its final stage when particles escape faster than they are replenished by the acceleration. It is tempting to consider SN 1006 as a prototype of such geometry, but the similarity is physically not quite convincing, given the young age of the latter source. On the other hand, older remnants, such as W44, do show a bipolar CR escape (Uchiyama et al. 2012) that can also be attributed to the field-aligned escape.

During earlier, more active stages of acceleration, CRs presumably fill up both the downstream and upstream regions near the shock. Meanwhile, the contact discontinuity (CD) behind the cloud of accelerated CRs must have undergone the Rayleigh–Taylor instability with strong magnetic field enhancement (Gull 1973). The CD expansion at late evolution stages should thus act as a piston on the previously accelerated CRs. Note that the CR reflecting piston was already employed in numerical acceleration schemes, e.g., Berezhko (1996), which might, however, overestimate the maximum CR energy (Kirk & Dendy 2001). In the post-acceleration stage, however, given

the significant field amplification at the CD, it is reasonable to assume that CRs are partially coupled to the slowly expanding flow with the reflecting magnetic piston behind, but while escaping upstream they couple to the ISM and diffuse away.

2.1. Basic Equations, Initial and Boundary Conditions

Perhaps the most systematic quasi-linear (QL) derivation of equations for the coupled evolution of CRs and Alfvén waves is given by Skilling (1975). We use them in a simplified one-dimensional (along the ambient field, z -coordinate, Figure 1) form equivalent to that used by, e.g., Bell (1978) and, with an interesting “beyond QL” interpretation, by Drury (1983),

$$\frac{d}{dt} P_{\text{CR}}(p) = \frac{\partial}{\partial z} \frac{\kappa_{\text{B}}}{I} \frac{\partial P_{\text{CR}}}{\partial z} \quad (1)$$

$$\frac{d}{dt} I = -C_{\text{A}} \frac{\partial P_{\text{CR}}}{\partial z} - \Gamma I. \quad (2)$$

Here, C_{A} is the Alfvén velocity, and the time derivative is taken along the characteristics of unstable Alfvén waves, forward propagating with respect to the flow of speed U :

$$\frac{d}{dt} = \frac{\partial}{\partial t} + (U + C_{\text{A}}) \frac{\partial}{\partial z}. \quad (3)$$

Equation (1) above is essentially a well-known convection–diffusion equation, written for the dimensionless CR partial pressure P_{CR} instead of their distribution function $f(p, t)$. We have normalized it to the magnetic energy density $\rho C_{\text{A}}^2/2$:

$$P_{\text{CR}} = \frac{4\pi}{3} \frac{2}{\rho C_{\text{A}}^2} v p^4 f, \quad (4)$$

where v and p are the CR speed and momentum, and ρ is the plasma density. The total CR pressure is normalized to $d \ln p$, similarly to the wave energy density I :

$$\frac{\langle \delta B^2 \rangle}{8\pi} = \frac{B_0^2}{8\pi} \int I(k) d \ln k = \frac{B_0^2}{8\pi} \int I(p) d \ln p.$$

Equation (2) is a wave kinetic equation in which the energy transferred to the waves equals the difference between the total work done by the particles, $(U + C_{\text{A}}) \nabla P_{\text{CR}}$, and the work done on the fluid, $U \nabla P_{\text{CR}}$ (Drury 1983). This interpretation of the wave generation indicates that it operates in a maximum efficiency regime. A formal QL derivation of this equation assumes that the particle momentum p is related to the wave number k by the “sharpened” resonance condition $kp = eB_0/c$ instead of the conventional cyclotron resonance condition $kp_{\parallel} = eB_0/c$ (note that here $k = k_{\parallel}$; Skilling 1975). We have included only the linear wave damping Γ and we will return to the possible role of nonlinear saturation effects later. We assume that $\partial P_{\text{CR}}/\partial z \leq 0$ at all times, so that only the forward propagating waves are unstable. The latter inequality is ensured by the formulation of initial value problem in each of the following two settings mentioned earlier in this section. In the first setting, the initial distribution of the CRC is symmetric with respect to $z = 0$, so we can consider their escape into the half-space $z > 0$. The second setting is when the cloud is limited from the left by a reflecting wall (CD). The appropriate boundary condition is $\partial P_{\text{CR}}/\partial z = 0$ at $z = 0$ in both cases.

Restricting our consideration to the case of coordinate-independent damping rate Γ , we obtain the following (“QL”)

integral of the system of Equations (1) and (2):

$$P_{\text{CR}}(z, t) = P_{\text{CR}0}(z') - \frac{\kappa_{\text{B}}}{C_{\text{A}}} \frac{\partial}{\partial z} \ln \frac{I(z, t)}{I_0(z')}. \quad (5)$$

Here, $P_{\text{CR}0}(z)$ and $I_0(z)$ are the initial distributions of the CR partial pressure and the wave energy density, respectively, and $z' = z - (U + C_{\text{A}})t$.

Using the QL integral, the system of Equations (1) and (2) can be reduced to one nonlinear convection–diffusion equation for, e.g., wave intensity $I(z, t)$. We will use dimensionless variables measuring the distance z in units of a_{\parallel} , which is the initial size of the CRC along the field line. The time unit is then a/C_{A} . Note, however, that, as the acceleration is assumed to be inactive, the particle momentum p enters the problem only as a parameter but, the initial scale height of the CRC a generally depends on p . It is also convenient to introduce a new variable for the wave energy density

$$W = \frac{C_{\text{A}} a(p)}{\kappa_{\text{B}}(p)} I \quad (6)$$

and similar relations for I_0 and W_0 . The equation for W then takes the following form:

$$\frac{\partial W}{\partial t} - \frac{\partial}{\partial z} \frac{1}{W} \frac{\partial W}{\partial z} = -\frac{\partial}{\partial z} \mathcal{P}_0(z). \quad (7)$$

We have neglected the wave propagation along the characteristics given by Equation (3) and the wave damping, assuming that these processes are slower than the CRC diffusion: $U, C_{\text{A}}, a\Gamma \ll \kappa_{\text{B}}/aI \sim cr_{\text{g}}/aI$. When the linear damping is important (e.g., in the case of Goldreich–Shridhar cascade, Farmer & Goldreich 2004), it can be easily incorporated into the current treatment by a simple change of variables indicated in Section 4. The function \mathcal{P} is defined similarly to W above,

$$\mathcal{P} = \frac{C_{\text{A}} a}{\kappa_{\text{B}}(p)} P_{\text{CR}}, \quad (8)$$

and, again, the index 0 refers in Equation (7) to the initial CR distribution $P_{\text{CR}0}(z)$. Thus, according to Equation (5), for the dimensionless CR partial pressure we have

$$\mathcal{P} = \mathcal{P}_0 - \frac{\partial}{\partial z} \ln \frac{W}{W_0}. \quad (9)$$

This quantity is governed by the equation

$$\frac{\partial \mathcal{P}}{\partial t} = \frac{\partial}{\partial z} \frac{1}{W} \frac{\partial \mathcal{P}}{\partial z}, \quad (10)$$

but its solution can be written down using the integral given by Equation (9), after the solution to Equation (7) is obtained.

While letting $C_{\text{A}} \rightarrow 0$ in the wave–particle collective propagation, we utilize the finiteness of C_{A} in determining the boundary condition for Equation (7) at $z = 0$ as follows. Returning from the nonlinear diffusion Equation (7) to Equation (2), one may see that the wave energy does not actually “diffuse” but it is generated locally by particles that diffuse. Had the neglected wave diffusion spread the waves to the point of their stability, viz., $z = 0$, they would be convected away from it by virtue of $C_{\text{A}} > 0$. Recalling the symmetry (reflection) boundary condition $\partial P_{\text{CR}}/\partial z = 0$ at $z = 0$ (no wave generation), we thus set a fixed boundary value $W(0, t) = W_0$, where W_0 is an initial (small) wave noise. It is instructive to investigate the

case in which the initial noise is the same throughout the entire half-space $z > 0$ (this limitation can be straightforwardly relaxed), so that the waves will be generated entirely by escaping particles, thus emphasizing the self-confinement. The second boundary condition is set by $W \rightarrow W_0$ for $z \rightarrow \infty$, and all $t < \infty$. Note that in general, $W_0 = W_0(p)$. These conditions determine the boundary value problem given by Equation (7) completely. However, we are interested primarily in diffusion of CRs outside the region of their initial localization, viz., at $z > 1$, where the source term in this equation vanishes. Therefore, the problem given by Equation (7) can be split into two separate problems, one in $0 \leq z \leq 1$ and another in $1 < z < \infty$ domain with the following junction conditions:

$$\frac{\partial}{\partial z} \ln W \Big|_{1-}^{1+} = W \Big|_{1-}^{1+} = 0. \quad (11)$$

These are the continuity conditions for both the wave energy density and pressure across the edge of the initial CR localization.

2.2. Self-similar Solution Outside the Region of Initial CR Localization

The nonlinear boundary value problem in the region $z > 1$ given by Equations (7) and (11) describes the CR propagation outside the region of their initial localization. This problem can be solved exactly using the following self-similar substitution:

$$W = \frac{1}{t^\alpha} w(\zeta), \quad \text{where } \zeta = \frac{z}{t^\beta}. \quad (12)$$

Submitting this to Equation (7) with $\mathcal{P}_0 = 0$ yields $\alpha = 2\beta - 1$. The boundary condition at infinity ($W \rightarrow W_0 \neq 0$, $z \rightarrow \infty$), on the other hand, requires $\alpha = 0$, so that the equation for w reads

$$\frac{d}{d\zeta} \frac{1}{w} \frac{dw}{d\zeta} + \frac{\zeta}{2} \frac{dw}{d\zeta} = 0, \quad (13)$$

with $\zeta = z/\sqrt{t}$. It is interesting to observe that this equation has a simple special solution $w = 2/\zeta^2 = 2t/z^2$. This solution describes a stationary particle distribution $\mathcal{P} \propto 1/z$ that is obviously related to the Bell (1978) asymptotic particle distribution in self-excited waves far away from a shock. In both cases, this is a singular limit of the problem as it implies a zero background turbulence level, $W_0 = 0$, and thus the number of particles in $z > 0$ half-space is infinite (Lagage & Cesarsky 1983; Drury 1983). Physically, this solution is different from what we find below in that it requires a permanent source of CRs at the origin so that their flux steadily drives waves that linearly grow in time.⁸ As we shall see, this simple special solution is an important singular limit of a more general and completely regular solution.

The general solution to Equation (13) can be found in quadratures by swapping ζ and w as dependent and independent variables and introducing an auxiliary function $V(w)$ by the following substitution:

$$\frac{dw}{d\zeta} = -\sqrt{2}w^{3/2}V(w). \quad (14)$$

⁸ There is no convection with the flow toward the origin ($U = 0$) in our case, which makes the solution unsteady, in contrast to the corresponding DSA problem (Bell 1978) where the solution is steady because of the convection, but the number of particles upstream is still infinite in both cases.

The equation for $V(w)$ takes the following form:

$$w \frac{d}{dw} w \frac{dV}{dw} + \frac{1}{4} \left(\frac{1}{V} - V \right) = 0. \quad (15)$$

This equation can be easily integrated, so that the function $w(\zeta)$ can be subsequently found from Equation (14). The first integral of Equation (15) is as follows:

$$\left(\frac{\partial V}{\partial \ln w} \right)^2 = R(V) \equiv \frac{1}{4}(V^2 - 2 \ln V - q), \quad (16)$$

where q is an integration constant. From Equation (14) and from the boundary condition $w \rightarrow W_0$ at $\zeta \rightarrow \infty$ we infer that $V(W_0) = 0$, so that from Equation (16) we find

$$w = W_0 e^{\int_0^V \frac{dV'}{\sqrt{R(V')}}}. \quad (17)$$

The function $w(\zeta)$ is then determined by the following relation for $\zeta(V)$, Equation (14):

$$\zeta = -\frac{1}{\sqrt{2}W_0} \int \frac{dV}{V\sqrt{R(V)}} e^{-\frac{1}{2} \int_0^V \frac{dV'}{\sqrt{R(V')}}}. \quad (18)$$

Using the identity $1/V = V - 2dR/dV$ and integrating Equation (18) by parts, after some manipulations the last equation simplifies considerably:

$$\zeta = \sqrt{\frac{2}{w}} (2\sqrt{R} + V). \quad (19)$$

It is useful to introduce an auxiliary constant V_1 related to the constant q and being the smaller of the two roots of $R(V)$, which is $R(V_1) = 0$. The requirement of a real zero of the function $R(V)$ ensures mapping two ‘‘copies’’ of the domain of V onto the full range $0 < \zeta < \infty$, whereby $\zeta \rightarrow \infty$ for $V \rightarrow 0$. Indeed, $\zeta(V)$ in Equation (19) diverges at $V = 0$ as $\sim \sqrt{-\ln V}$. However, increasing V from $V = 0$ to $V = V_1$ does not cover the full range $0 < \zeta < \infty$ yet, as may be seen from Equation (19); ζ decreases from ∞ only to $\zeta_1 \equiv V_1 \sqrt{2/w(V_1)} > 0$. To continue the integral curve to $\zeta = 0$, it is necessary to switch branches of \sqrt{R} at $V = V_1$ in Equations (17) and (19) and so continue the integral in Equation (17) back to $V < V_1$ (along the second copy of the V -domain). Decreasing then V from $V = V_1$ to $V = V_0 \equiv \exp(-q/2)$ brings the integral curve to the point $\zeta = 0$, $w = w_{\max} = w(\zeta = 0)$ (Figure 2). The explicit formal representation of the general solution of Equation (13) is given in Appendix A along with a numerical example (Figure 3). Equations (17) and (19) determine the solution $w(\zeta)$, where the integration constant V_0 (or q) should be obtained from the matching condition, Equation (11). This can be done by considering Equation (7) inside the region of initial CR localization, i.e., $0 < z < 1$, where its right-hand side is nonzero.

2.3. Solution Inside the Initial CR Cloud

Given an initial distribution $\mathcal{P}_0(z)$, Equation (7) can always be integrated numerically in the finite domain $0 < z < 1$, so that the full solution will be obtained from the boundary conditions and from the results of the previous section. However, according to Equation (10), already for $t \gtrsim W_0$, where $W_0 \ll 1$, the initial profile $\mathcal{P}_0(z)$ will be redistributed over the unity interval in such

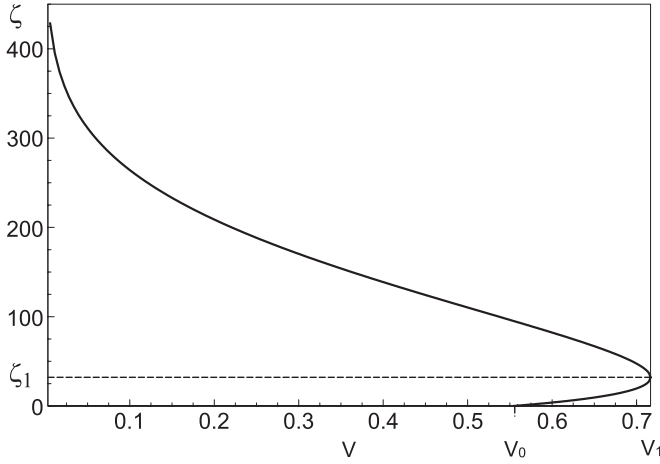


Figure 2. Two branches of function $\zeta(V)$, Equation (A4), depicted for $\varepsilon = 0.3$. Note that $R(V=0) = \infty$, $R(V_0) = V_0/4$, $R(V_1) = 0$, and $\zeta(V_0) = 0$ on the lower branch of $\zeta(V)$.

a way as to approach a quasi-steady state in which the flux $W_0^{-1} \partial W / \partial z$ in Equation (7) through $z = 0$ will be balanced by the source integral, $\mathcal{P}_0(0)$ (recall that $\mathcal{P}_0(1) = 0$). The particle flux through the $z = 1$ boundary decays as $t^{-1/2}$ with time (since $|\partial w / \partial \zeta| < \infty$ at $\zeta \rightarrow 0+$; see the preceding section or Equation (23) below). Therefore, for the self-similar stage of the cloud relaxation we can write

$$\ln \frac{W}{W_0} = \int_0^z \mathcal{P}_0 dz - B(t)z, \quad (20)$$

where the “integration constant” B depends slowly (in the above sense) on time. Using the first matching condition in Equation (11), i.e., the CR pressure continuity, we can specify $B(t)$ as follows: $B \propto t^{-1/2} \rightarrow 0$ as $t \rightarrow \infty$ (see Equation (23) below). This determines the self-similar (outer, $z > 1$) solution by the second matching condition in Equation (11):

$$w(0) \equiv \lim_{t \rightarrow \infty} w \left(\frac{1}{\sqrt{t}} \right) = w_{\max} = W_0 e^\Pi. \quad (21)$$

Here we have introduced the integrated partial pressure as follows:

$$\Pi = \int_0^1 \mathcal{P}_0 dz. \quad (22)$$

The function $B(t)$ and thus the internal solution $W(z, t)$ in Equation (20) may be obtained using this equation, the first matching condition in Equation (11), and Equation (14),

$$B(t) = -\frac{1}{\sqrt{t}} \frac{\partial}{\partial \zeta} \ln w \Big|_{\zeta=1/\sqrt{t}} = \sqrt{2w/t} V \Big|_{\zeta=1/\sqrt{t}}. \quad (23)$$

Note that the particle pressure at $z > 1$ is completely determined by the turbulence level w , Equation (9).

Now we can determine the integration constant q introduced in the preceding section. From Equations (21) and (A3) we obtain the following equation for q :

$$\int_0^{V_1} dV / \sqrt{R(V)} + \int_{V_0}^{V_1} dV / \sqrt{R(V)} = \Pi, \quad (24)$$

where $R(V_1) = 0$, $R(V_0) = -V_0/2$, while $R(V)$ is given by Equation (16). In the most interesting case $q \approx 1$, it is convenient

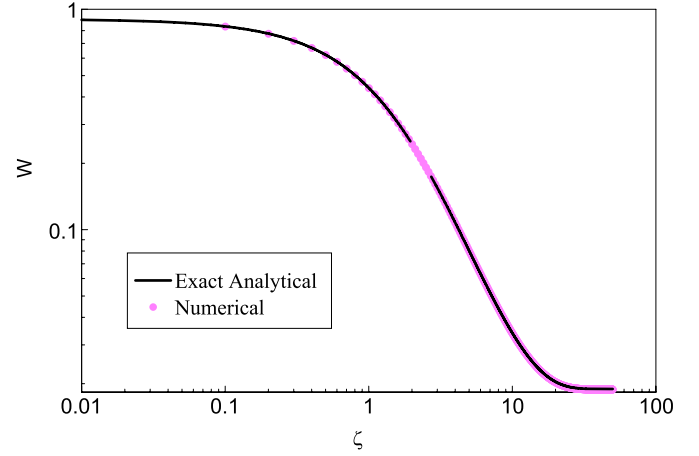


Figure 3. Analytic vs. numerical solution of Equation (14). The gap in the analytical curve encloses the branching point of the solution at $V = V_1$ (Equation (A1)). $w_0 = 0.19$, $w_m = 0.9$.

(A color version of this figure is available in the online journal.)

to use the constant $\varepsilon^2 = (q - 1)/2$ in place of q . In this case, $\Pi \gg 1$, $\varepsilon \ll 1$, $V_1 \approx 1 - \varepsilon$, and

$$\begin{aligned} \Pi &= 2 \int_0^{V_1} \frac{dV}{\sqrt{R}} \approx 2^{3/2} \int_0^{1-\varepsilon} \frac{dV}{\sqrt{(V-1)^2 - \varepsilon^2}} \\ &\approx 2^{3/2} \ln \frac{2}{\varepsilon} + \mathcal{O}(1), \end{aligned}$$

so that the turning point of the solution at $V = V_1$ approaches the critical point $V = 1$, where R has a minimum (Figure 2)

$$V_1 = 1 - 2e^{-\Pi/2\sqrt{2}}.$$

For $\Pi \ll 1$, we can write instead, $V_1 \approx V_0(1 + V_0^2/2)$ where $V_0 = \exp(-q/2)$.

To conclude this section, the self-similar expansion of the CRC described by Equations (7)–(10) is controlled by two parameters. One parameter is the background turbulence level $W_0(p)$ in the media into which the cloud expands. The second parameter is the integrated pressure of the cloud, Π . Although the initial wave energy density inside the cloud ($z < 1$) is likely to be higher than W_0 , we have adopted the background value W_0 also inside the cloud for simplicity, as this should not influence the self-similar CR propagation outside the cloud. In addition, efficient wave generation by a dense expanding CRC renders the initial value for the wave energy density inside the CRC unimportant.

3. ANALYSIS OF THE SOLUTION

Once we have the solutions outside and inside the region of initial CR localization, we may precisely calculate how fast particles escape from this region. Two convenient characteristics of the escape process are the half-life time and the width of the CR distribution. We begin our analysis of the solution from computing these simple quantities and turn to the details of the CR escape afterward.

3.1. Half-life Time and the Width of the CR Cloud

The most concise characterization of the escape may be given by looking at the following two parts of the (conserved) integral

particle pressure:

$$\Pi = \Pi_0 + \Pi_1 = \text{const},$$

where

$$\Pi_0 = \int_0^1 \mathcal{P} dz \text{ and } \Pi_1 = \int_1^\infty \mathcal{P} dz$$

refer to the regions inside and outside of the initial CRC, respectively. Recall that at $t = 0$, $\Pi_0 = \Pi$ and $\Pi_1 = 0$, while at $t = \infty$, an opposite CR distribution is reached: $\Pi_0 = 0$ and $\Pi_1 = \Pi$. Note that Equation (21) specifies the total work ultimately done by particles on waves, while they diffuse from $0 < z < 1$ to $1 \leq z < \infty$. As Π is conserved, it is natural to define the CR confinement time as the time at which Π_0 (Π_1) drops (raises) to a half of Π . Substituting W from Equation (12) into Equation (9), we obtain

$$\Pi_1(t) = \ln \left. \frac{w}{W_0} \right|_{\zeta=1/\sqrt{t}}.$$

For the half-life time $t = t_{1/2}$ we may use the following equations:

$$\Pi_1(t_{1/2}) = \Pi_0(t_{1/2}) = \frac{1}{2}\Pi. \quad (25)$$

In the simple TP case ($\Pi \ll 1$), the half-life time amounts to (see Appendix B)

$$t_{1/2} \approx \frac{1}{4\sigma} W_0 \quad (26)$$

with $\sigma \approx 0.23$. In the opposite case $\Pi \gg 1$, for $t_{1/2}$ we obtain

$$t_{1/2} \approx t_1 = 1/\zeta_1^2 \equiv \frac{w_1}{2V_1^2} \approx \frac{w_1}{2} \quad (27)$$

(see Equation (19)). Note that for $\Pi \gg 1$, $V_1 \approx V_{1/2}$ (see Appendix B), and for the half-life time we obtain

$$t_{1/2} = \frac{1}{2} W_0 e^{\Pi/2}. \quad (28)$$

It is clear that the nonlinear delay factor $\exp(\Pi/2)$ slows down the escape considerably, compared to the TP solution.

Another important characteristic of the particle escape is the spatial width of their distribution. Formally, the self-similar solution is scale-invariant $\sim 2/\zeta$, for $\Pi \gg 1$ over the most part of the spatial distribution of the partial pressure (see below). Therefore, to characterize the width we use the point $\zeta_{1/2}$, related to the half-time $t_{1/2}$, as follows:

$$\zeta_{1/2} = \frac{1}{\sqrt{t_{1/2}}} = \sqrt{\frac{2}{W_0}} e^{-\Pi/4}.$$

In physical coordinate z , this point moves outward as $z_{1/2} = \zeta_{1/2} \sqrt{t}$ starting from $z = 1$ at $t = t_{1/2}$. The expansion rate of a dense CRC ($\Pi \gg 1$) is thus exponentially low.

3.2. Spatial Distribution of the CR Cloud

Considering the spatial distribution of the spreading CRC in detail, it is convenient to start with the region far away from the source, where $W \rightarrow W_0$. This asymptotic behavior corresponds to the case $V \ll 1$. Introducing an auxiliary function $U(\zeta)$,

$$U = -\frac{\partial}{\partial \zeta} \ln w = \sqrt{2w} V, \quad (29)$$

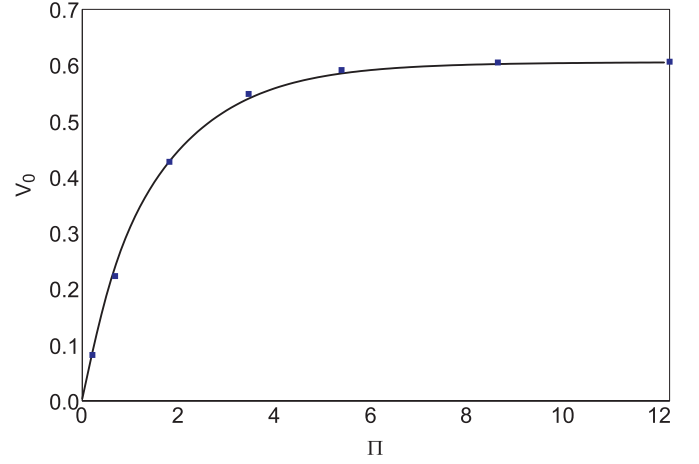


Figure 4. Squares: function $V_0(\Pi)$, obtained from Equation (24). Line: interpolation given by Equation (32).

(A color version of this figure is available in the online journal.)

that is related to the particle pressure through $\mathcal{P} = U(\zeta)/\sqrt{t}$, and using Equations (16) and (19), we obtain for U the following expression:

$$U(\zeta) = \sqrt{2W_0} V_0 e^{-W_0 \zeta^2/4}. \quad (30)$$

Therefore, the asymptotic CR pressure depends on the following two parameters: the ISM background diffusivity $W_0^{-1}(p) \equiv W^{-1}(p, z = \infty)$ (see Equation (10)) and on the CR source pressure $\Pi(p)$, but only through the parameter $V_0 = \exp(-q/2)$. The latter grows linearly with $\Pi \ll 1$ but it saturates when $\Pi \gg 1$:

$$V_0 \approx \begin{cases} \frac{1}{\sqrt{2\pi}} \Pi, & \Pi \ll 1 \\ \exp\left(-\frac{1}{2} - 4e^{-\Pi/\sqrt{2}}\right), & \Pi \gg 1. \end{cases} \quad (31)$$

For practical calculations, it is more convenient to combine both asymptotic regimes into the following simple interpolation formula:

$$V_0 = \left[(\sqrt{2\pi}/\Pi)^{5/2} + \left(\sqrt{e} + \frac{3}{2} e^{-\Pi/\sqrt{2}} \right)^{5/2} \right]^{-2/5} \quad (32)$$

which not only recovers both $\Pi \ll 1$ and $\Pi \gg 1$ regimes but also reproduces the transition zone accurately. The latter property is achieved by the choice of numerical parameters of the interpolation, i.e., the powers 5/2, 3/2, and $-2/5$. The quality of the interpolation may be seen from Figure 4, where the formula in Equation (32) is shown against exact numerical points calculated from Equation (24). The partial pressure $\mathcal{P}(z, t)$ is then given by

$$\mathcal{P} = U/\sqrt{t} = \sqrt{2W_0/t} V_0(\Pi) e^{-W_0 z^2/4t}. \quad (33)$$

Note that for strong sources ($\Pi \gg 1$) the CR density at large distances becomes independent of the source strength. This is the regime of an efficient ablative escape suppression in which a small (and Π -independent!) number of leaking particles leave behind enough Alfvén fluctuations to limit the leakage of particles remaining in the source to exactly the rate given by Equation (33).

The spatial distribution of the CRs becomes even more universal closer to the origin where it falls off as $\mathcal{P} \approx 2/z$ before

it turns into an innermost flat-top part of the entire distribution for $\zeta^2 < D_{\text{NL}}(p)$. We have introduced the “self-confinement” diffusion coefficient D_{NL} as

$$D_{\text{NL}} = \frac{2}{V_0^2} D_{\text{ISM}} e^{-\Pi} = \frac{2}{V_0^2 w_{\text{max}}} \quad (34)$$

with $D_{\text{ISM}} = W_0^{-1}$. To obtain this intermediate ($D_{\text{NL}} < \zeta^2 < D_{\text{ISM}}$) part of the CR spatial distribution, we expand the analytic solution given by Equations (17) and (19) in small $V_1 - V \ll 1$. Using the expression for the self-similar CR pressure U from Equation (29) we obtain the following expansion near $\zeta = \zeta_1 \equiv \zeta(V_1)$:

$$U = \frac{2}{\zeta} \left[1 - \frac{3\epsilon}{2} \left(\frac{2}{w_1} \right)^{2-3/2} \zeta^{-\sqrt{2}} - \frac{\epsilon}{2} \left(\frac{w_1}{2} \right)^{2-3/2} \zeta^{\sqrt{2}} \dots \right], \quad (35)$$

where $w_1 = 2V_1^2/\zeta_1^2$, and $\epsilon \equiv (q-1)/2$. Note that while the solution has a branching point in auxiliary variable V at $V = V_1$, it is a regular and single-valued function of the physical variable ζ , throughout the entire half-space $\zeta > 0$, including the branching point of $\zeta(V)$ at $V = V_1$, as it should be. We also notice that while ζ decreases starting from ζ_1 , the solution grows slower than $1/\zeta$, leveling off toward the origin. The above expansion, however, becomes inaccurate for smaller ζ and we alter it below.

Now we turn to this innermost part of the distribution where the particle diffusion coefficient is most strongly decreased. It is convenient to expand the solution in a series in $\xi \equiv V/V_0 - 1 \ll 1$. Using the representation of w given by Equation (A2), we obtain

$$w = w_{\text{max}} \left[\frac{\xi - a + \sqrt{\xi^2 - 2a\xi + b^2}}{b - a} \right]^{-2b},$$

where $a = (1 - V_0^2)/(1 + V_0^2)$ and $b = V_0/\sqrt{1 + V_0^2}$. Then, using the expression (A4) for small ζ and Equation (29), we obtain for $U(\zeta) = \mathcal{P}\sqrt{t}$ the following simple result:

$$U \approx \frac{\sqrt{2w_{\text{max}}} V_0}{1 + w_{\text{max}} \zeta^2/4} \approx \sqrt{2w_{\text{max}}} V_0 e^{-w_{\text{max}} \zeta^2/4}, \quad (36)$$

valid for $w_{\text{max}} \zeta^2 \lesssim 1$. Note that we have rewritten, with the same accuracy, the denominator in the standard “diffusion” form, $\exp(-w_{\text{max}} \zeta^2/4)$, which shows that the CR diffusivity is diminished by a factor $W_0/w_{\text{max}} = \exp(-\Pi) \ll 1$ compared to its background level W_0^{-1} . If, however, $w_{\text{max}} \gtrsim aC_A/\kappa_B$ (see Equation (6)), a better approximation would be to simply replace the diffusion coefficient by its Bohm value, as the neglected nonlinear wave interactions (see Section 4) should render $\delta B \sim B_0$. The result in Equation (36) should then be replaced by

$$U = \sqrt{2aC_A/\kappa_B} V_0(\Pi) e^{-aC_A \zeta^2/4\kappa_B t}. \quad (37)$$

Equations (30), (35), and (36) provide the *explicit* asymptotic representation of the exact *implicit* solution given by Equations (17) and (19). This representation is rigorous but somewhat impractical, so we provide, again, an interpolation formula that accurately describes the solution $U(\zeta) = \mathcal{P}\sqrt{t}$ in the entire range of $0 < \zeta < \infty$ (Figure 5),

$$U = 2[\zeta^{5/3} + (D_{\text{NL}})^{5/6}]^{-3/5} e^{-W_0 \zeta^2/4}, \quad (38)$$

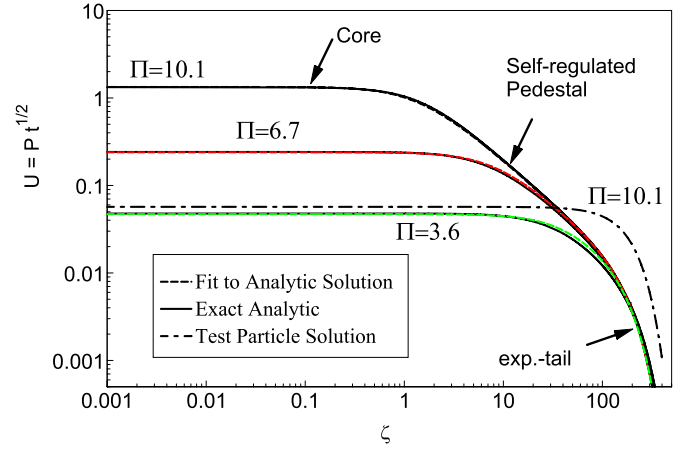


Figure 5. Spatial distribution of CR partial pressure (as a function of $\zeta = z/\sqrt{t}$, multiplied by \sqrt{t}) shown for integrated values of this quantity $\Pi = 3.6; 6.7; 10.1$ and for the background wave amplitude $W_0 = 10^{-4}$. Exact analytic solutions are shown with the solid lines while the interpolations given by Equation (38) are shown with the dashed lines. For comparison, a formal linear solution for $\Pi = 10.1$ is also shown with the dot-dashed line. Note the three characteristic zones of the CR confinement: the innermost flat-top core, the scale-invariant ($1/\zeta$) pedestal, and the exponential decay zone.

(A color version of this figure is available in the online journal.)

where $D_{\text{NL}}(\Pi)$ is defined in Equation (34) with V_0 given by the interpolation in Equation (32). The last formula recovers the limiting cases given by Equations (30), (35), and (36) except a slight modification of Equation (30) at large ζ , so that an extra $1/\zeta$ -factor is accepted in the interests of parameterization simplicity. According to Figure 5, however, this deviation from the correct asymptotic expansion of the exponential tail of the distribution is not really noticeable.

The overall profile of the partial pressure presented in log–log format (Figure 5) unveils the CR escape as a highly structured process. It comprises a nearly flat-top core (Equation (36)), a nearly $1/\zeta$ pedestal (Equation (35)), and an exponential foot (Equation (30)). We already noted that the escape rate of CR in the foot saturates with the source strength for $\Pi \gg 1$. This is easy to understand as the foot is separated from the core (source) by the flux controlling pedestal, where the CR transport is self-regulated in such a way that a fixed CR flux streams through it to the foot regardless of the strength of the CR source. The solution is shown in Figure 5 as a function of ζ using the self-similar variables $U = \mathcal{P}\sqrt{t}$ and $\zeta = z/\sqrt{t}$. Remarkably, the pedestal portion of the profile does not change with time also in the physical variables, \mathcal{P}, z : $\mathcal{P} \approx 2/z$. The core, however, sinks in as $\mathcal{P} \propto 1/\sqrt{t}$, but in addition, it expands in z as $\sqrt{D_{\text{NL}} t}$, to conserve the integrated pressure contained in the core at the expense of the pedestal that shrinks accordingly. The latter disappears completely at $t \sim D_{\text{ISM}}/D_{\text{NL}}$, after which the further escape proceeds in a TP regime but with a smaller diffusion coefficient in the core–pedestal region, since waves persist even after most of particles have escaped. At this point, the wave damping should become important (see Section 4).

As the TP approximation is widely used in calculating the CR escape from their sources, we also show, for comparison, one such example in Figure 5. We plot the following simple TP solution

$$U = \sqrt{\frac{W_0}{\pi}} \Pi e^{-W_0 \zeta^2/4} \quad (39)$$

that can be obtained from Equation (38) or Equation (33) with $V_0(\Pi)$ taken from Equation (31) or Equation (32) for

$\Pi \ll 1$. To compare the self-regulated escape with the TP one, we formally extend the above solution to large Π , as this is normally done within TP approaches. Such an extension clearly underestimates the nonlinear level of the CR pressure by a factor $\sim \Pi^{-1} \exp(\Pi/2) \gg 1$ in the core and in the most of the pedestal. By virtue of lacking self-regulation, it also overestimates the pressure in the exponential foot by a factor $\Pi \gg 1$.

3.3. Control Parameters and Predicted CR Flux in Physical Units

The integrated partial pressure Π is the most important parameter that regulates the CR escape. Therefore, we consider it in some detail, returning to the dimensionful variables and rewriting Π as follows (see Equations (8) and (22)):

$$\Pi \simeq 3 \frac{C_A}{c} \frac{a(p)}{r_g(p)} \frac{\bar{P}_{\text{CR}}(p)}{B_0^2/8\pi}, \quad (40)$$

where $a(p)$ is the initial size of the CRC, r_g is the CR gyroradius, and $\bar{P}_{\text{CR}}(p)$ is their average partial pressure inside the cloud. Although the ratio of Alfvén speed to speed of light, C_A/c , is typically very small ($\sim 10^{-5}$ to 10^{-4}), the remaining two ratios in the last equation may be fairly large. Indeed, a/r_g should amount to several $c/U_{\text{ST}} \gg 1$, with U_{ST} being the shock speed at the end of the ST stage, as a should exceed the precursor size cr_g/U_{ST} . Indeed, a significant part of the shock downstream region filled with CR, which have been convected there over the entire history of CR production, may significantly contribute to, if not dominate, the total size of the cloud a (Kang et al. 2009). This is particularly relevant to the CR release during the decreasing maximum energy (reverse acceleration phase; Gabici 2011). In the forward acceleration regime (growing maximum energy) Bohm diffusion, the downstream CR scale height is similar to that of the upstream. A reasonable estimate for U_{ST} is $c/U_{\text{ST}} \gtrsim 10^3$. Finally, the CR pressure in the source should considerably exceed the magnetic pressure as both quantities are roughly in equipartition in the background ISM. Alternatively, as is usually assumed, the accelerated electrons are in equipartition with the magnetic energy inside the source, since they should have lost their excessive energy via synchrotron radiation. As electrons are thought to be involved in the acceleration at $\sim 10^{-2}$ of the proton level, the last ratio in Equation (40) is then $\sim 10^2$, thus giving, perhaps, an upper bound to the pressure parameter $\Pi \sim 10^2/M_A$, where $M_A = U_{\text{ST}}/C_A$.

One of a few other ways the parameter Π can be looked at is to express it through the average acceleration efficiency $\mathcal{E} = 2\bar{P}_{\text{CR}}/\rho\bar{U}^2$, where \bar{U} is the shock velocity, appropriately averaged over the CR acceleration history (one may expect $\bar{U} \gg U_{\text{ST}}$). Then $\Pi \simeq 3(\bar{U}^2/cC_A)(a/r_g)\mathcal{E} \simeq 3A(\bar{U}^2/U_{\text{ST}}C_A)\mathcal{E}$, where we have introduced a factor $A = (a/r_g)U_{\text{ST}}/c \gtrsim 1$. In this form, the estimate indeed boils down to the acceleration efficiency \mathcal{E} with the remaining quantities (A , \bar{U} and U_{ST}) being more accessible to specific models. Since the acceleration efficiency \mathcal{E} is believed to be at least $\gtrsim 0.1$ for productive SNRs, we conclude that the control parameter Π is rather large than small. The caveat here is that it might, in some cases, be too large to limit the applicability of the above treatment. We return to this issue in the Discussion section.

Once the major control parameter is known, we can calculate the distribution function f_{CR} of the CR, released into the ISM, depending on the distance from the source z and time, using the parameterization in Equation (38). It is convenient to rewrite it

in the form of the CR partial pressure \hat{P}_{CR} in physical units as follows:

$$\frac{\hat{P}_{\text{CR}}}{B_0^2/8\pi} \simeq 0.8 \left(\frac{M_A}{A} \frac{10^4 \text{ yr}}{t} \frac{n}{1 \text{ cm}^{-3}} \frac{E}{1 \text{ GeV}} \right)^{1/2} \left(\frac{1 \mu\text{G}}{B} \right)^{3/2} U(\zeta). \quad (41)$$

Here, $M_A = U_{\text{ST}}/C_A$, n is the plasma number density, E is the particle energy, and B is the magnetic field. The self-similar coordinate ζ can be represented, in turn, in the following way:

$$\zeta \simeq 17 \left(\frac{M_A}{A} \frac{1 \text{ GeV}}{E} \frac{B}{1 \mu\text{G}} \frac{10^4 \text{ yr}}{t} \right)^{1/2} \frac{z}{\text{pc}}. \quad (42)$$

Once this quantity is calculated for given z and t , the CR partial pressure in Equation (41) can be obtained from Equation (38) or from Figure 5. Note that the scale of the CR pressure is determined by the maximum of $U = U(0) = \sqrt{2}W_0V_0 \exp(\Pi/2)$, where V_0 is given by Equation (32). The CR partial pressure also depends on the energy through W_0 and Π , apart from the factor \sqrt{E} in Equation (41), which will be discussed below. Finally, the background diffusion coefficient of CR in physical units is related to the dimensionless diffusivity W_0^{-1} as follows:

$$D_{\text{ISM}} = 6.6 \times 10^{27} \frac{10^{-4}}{W_0} \frac{a}{1 \text{ pc}} \frac{B}{1 \mu\text{G}} \left(\frac{1 \text{ cm}^{-3}}{n} \right)^{1/2} \text{ cm}^2 \text{ s}^{-1}.$$

3.4. The Form of the Spectrum of Escaping CR

As the transition from the flat-top part of the normalized (Equation (8)) partial pressure $\mathcal{P}(p)$ to the pedestal is described by a function $\mathcal{P} \approx 2\{z^{5/3} + [D_{\text{NL}}(p)t]^{5/6}\}^{-3/5}$, the pressure $\mathcal{P}(p)$ is almost p -independent (the corresponding particle momentum distribution $f_{\text{CR}} \propto \kappa_B p^{-4}/\hat{z}$, in the physical units, $\hat{z} = az$) for such momenta where $D_{\text{NL}}(p) < z^2/t$, for the fixed dimensionless observation point z and time t . At $p = p_{\text{br}}$, where $D_{\text{NL}}(p_{\text{br}}) = z^2/t$, the spectrum incurs a break. If we approximate $D_{\text{NL}} \propto p^\delta$ near $p \sim p_{\text{br}}$, the break will have an index $\delta/2$, as may be seen from the above formula for \mathcal{P} . The index δ thus derives from the momentum dependence of the $D_{\text{ISM}}(p)$ and from that of the coordinate-integrated CR pressure $\Pi(p)$ (through the factor $\exp(-\Pi)$ in Equation (34)). Furthermore, if we represent $\exp(-\Pi) \propto p^{-\sigma}$ and $D_{\text{ISM}} \propto p^\lambda$ at $p \sim p_{\text{br}}$, so that $\delta = \lambda - \sigma$, then \mathcal{P} is flat at $p < p_{\text{br}}$ for $\delta > 0$ and steepens to $p^{-\delta/2}$ at $p = p_{\text{br}}$. Conversely, if $\delta < 0$, \mathcal{P} raises with p as $p^{-\delta/2}$ at $p < p_{\text{br}}$ and it levels off at $p > p_{\text{br}}$. Note, however, that Π is momentum independent in the important case of the p^{-4} distribution of the initial CRC with the scale height $a(p) \propto \kappa_B$. This case corresponds to the TP DSA spectrum, $\propto p^{-4}$ with a scale height a estimated from the shock precursor size. The break has then an index $\lambda/2$ and it is entirely due to the D_{ISM} momentum dependence.

4. COMPARISON WITH OTHER APPROACHES

Given the variety of approaches to the CR escape, we extend our brief discussion in the Introduction section by putting our treatment into perspective. Most of the approaches can be categorized into the following three kinds. First of all, a simple TP approach is feasible for a rarefied CRC, when wave generation is negligible (e.g., Aharonian & Atoyan 1996; Drury 2011; Ohira et al. 2011). It solves the linear diffusion equation for the CRs with a diffusion coefficient determined by a given (e.g., background) turbulence. Next, there are

modifications of this approach that include the wave generation by escaping particles balanced by the MHD cascades (e.g., Ptuskin & Zirakashvili 2005; Ptuskin et al. 2008; Yan et al. 2012). The wave intensity, thus obtained, is then used to calculate the particle diffusion coefficient and their distribution. We call these approaches modified TP, as they do not evolve waves but slave them to the instant particle distribution. The third treatment is based on a QL mechanism, whereby the wave stabilization primarily occurs through their back-reaction on the particles (e.g., suppression of instability by pitch-angle isotropization). The nonlinear effects may or may not be significant during the QL stabilization. As the QL wave saturation operates at the lowest order in wave energy, it is imperative to consider it first, particularly where the waves become weaker. This approach has been well tested on the somewhat similar problem of a hot electron cloud expansion into a plasma (Ryutov & Sagdeev 1970; Ivanov et al. 1970). In the case of a CRC expansion into the ISM, there is an extended region (i.e., “pedestal” self-confinement region) where the level of turbulence significantly exceeds the background but is still not high enough for the nonlinear effects to dominate over the QL ones. As our results show, this is the most important domain that determines the spectrum of escaping CRs. Simply put, the dynamics is dominated by wave generation and self-regulated particle escape, rendering the nonlinear wave dynamics and MHD cascades less important. It should be noted, however, that the instability driving pitch-angle anisotropy is supported by the spatial inhomogeneity of the CRC, so that the full stabilization occurs (under negligible damping) only when particles spread to infinity.

It is nonetheless worthwhile to consider the possible effect of wave damping we have neglected. For example, Ptuskin et al. (2008), while neglecting dI/dt on the left-hand side of Equation (2), balance the driving term with the damping term on its right-hand side and assume a Kolmogorov dissipation for Γ ,

$$\Gamma = kC_A\sqrt{I}/(2C_K)^{3/2} \quad (43)$$

with $C_K \approx 3.6$ and $k \simeq 1/r_g(p)$ being the resonant wave number. Therefore, only Equation (1) needs to be solved. The CR density decays then at the source as $\propto t^{-3/2}$ and the flat-topped, self-confined part of the CR distribution spreads as $z \propto t^{3/2}$, both pointing at the superdiffusive CR transport.⁹ The reason is clearly in a very strong wave damping due to the Kolmogorov dissipation. For the same reason this solution does not recover the TP asymptotic $P_{CR} \propto t^{-1/2} \exp(-z^2/4D_{ISM}t)$, physically expected in $z, t \rightarrow \infty$ limit in the ISM with the background diffusion coefficient D_{ISM} . While such a strong wave damping may be justified in the core of the CRC during the early phase of escape, the overall confinement is controlled by the $1/z$ -pedestal, where the waves are relatively weak and the Kolmogorov cascade can hardly be important. Moreover, since the pedestal plays a role of a barrier enclosing the core, the wave-particle interaction dynamics in the core is less important than that in the pedestal. In this regard, the particle distribution in the core is similar to the QL plateau on particle distribution in momentum space. When established, the plateau does not depend on the interaction of the waves that create it.

An alternative choice of damping mechanism is the Goldreich & Sridhar (1997, hereafter GS) MHD cascade, which seems to be more appropriate in $I \lesssim 1$ regime (Farmer & Goldreich

2004; Beresnyak & Lazarian 2008; Yan et al. 2012) and may play some role in the pedestal. The damping rate is

$$\Gamma = C_A\sqrt{\frac{k}{L}}, \quad (44)$$

where L is the outer scale of turbulence which may be as large as 100 pc. Not only is this damping orders of magnitude (roughly a factor $\sqrt{L/r_g}$) lower than the Kolmogorov one, but it does not depend on I and can be considered as coordinate independent. Then, the damping term does not violate the QL integral, Equation (5). The dimensionless Equation (7) can thus be rewritten simply as follows (outside the initial CRC):

$$\frac{\partial W}{\partial t} = \frac{\partial}{\partial z} \frac{1}{W} \frac{\partial W}{\partial z} - \Gamma' W,$$

and the dimensionless damping $\Gamma' = a/\sqrt{r_g}L \sim (c/U_{ST})\sqrt{r_g}/L$ may be eliminated by replacing $W \exp(\Gamma't) \rightarrow W$, $\int_0^t \exp(\Gamma't) dt \rightarrow t$. Our results then remain intact in the relabeled t and W .

The above three approaches to the CR escape are summarized in Figure 6. The key ingredients are the CR particles and Alfvén waves while the relevant physical phenomena are the wave-particle and wave-wave interactions. Under the latter one may loosely understand both weakly turbulent parametric processes (such as wave decay) and turbulent cascades similar to those described above. The wave-particle interactions comprise the unstable growth of Alfvén waves together with their back-reaction on the CRs. In principle, the wave-wave interactions need to be included in the QL treatment, particularly in the core of the CRC when $w_{\max} \gtrsim 1$. However, as the wave dynamics in the flat core is relatively unimportant, one may employ the Bohm diffusion coefficient in this region, i.e., where $z^2/t \lesssim D_{NL}$ by setting $D_{NL} \sim \kappa_B$ and thus obtain a result already given by Equation (37). Formally, it is equivalent to the TP approximation with the minimum diffusion coefficient set at the Bohm level.

To summarize our results, we have considered the self-consistent relaxation of a CRC injected into a magnetized plasma (ISM) under the assumption of an initially weak background turbulence, $(\delta B/B_0)^2 \ll 1$, so that the cross-field diffusion is negligible, $\kappa_{\perp} \ll \kappa_{\parallel}$ outside the cloud and the particles escape largely along the field, i.e., in z -direction. The principal parameter that regulates the CR escape from the cloud is identified to be the coordinate-integrated partial pressure Π , given, e.g., in Equation (40). Resonant waves of the length $\sim r_g^{-1}(p)$, driven by the run-away cloud particles, are found to confine the core CRs very efficiently when $\Pi \gg 1$.

The resulting normalized (Equation (8)) CR partial pressure profile \mathcal{P} comprises the following three zones: (1) a quasi-plateau (core) at $z/\sqrt{t} < \sqrt{D_{NL}}$ of a height $\sim (D_{NL}t)^{-1/2}$, which is elevated by a factor $\sim \Pi^{-1} \exp(\Pi/2) \gg 1$, compared to the TP solution because of the strong QL suppression of the CR diffusion coefficient with respect to its background (TP) value D_{ISM} : $D_{NL} \sim D_{ISM} \exp(-\Pi)$; (2) next to the core, where $\sqrt{D_{NL}} < z/\sqrt{t} < \sqrt{D_{ISM}}$, the profile is scale invariant, $\mathcal{P} \approx 2/z$. The CR distribution in this “pedestal” region is fully self-regulated and independent of Π and D_{ISM} for $\Pi \gg 1$; (3) the tail of the distribution at $z/\sqrt{t} > \sqrt{D_{ISM}}$ is similar in shape to the TP solution but it saturates with $\Pi \gg 1$, so that the CR partial pressure is $\propto (D_{ISM}t)^{-1/2} \exp(-z^2/4D_{ISM}t)$, independent of the strength of the CR source Π , in contrast to the TP result that scales as $\propto \Pi$.

⁹ Recall that our results give for these quantities $t^{-1/2}$ and $t^{1/2}$, respectively.

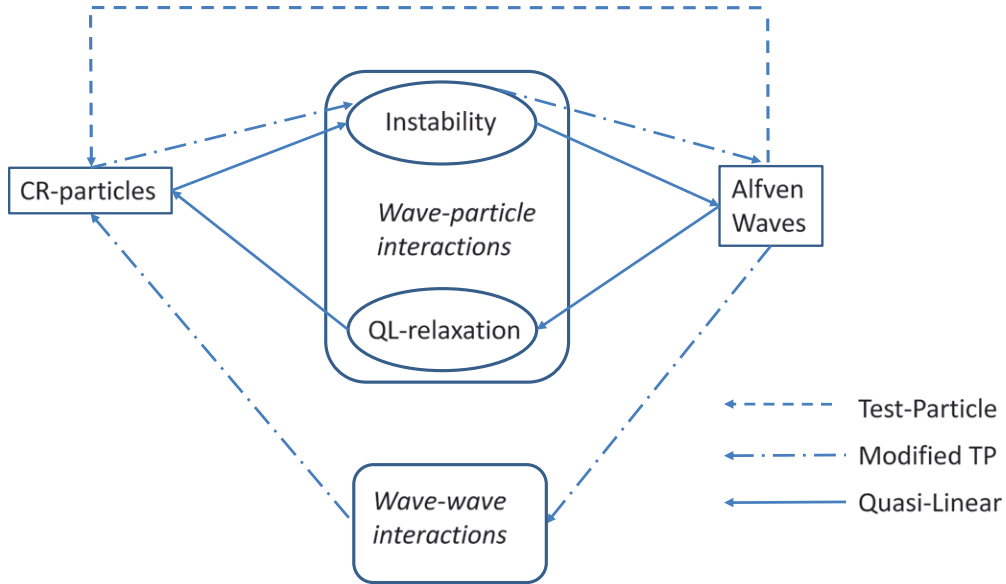


Figure 6. Three different approximations for studying injection of accelerated CRs into ISM: test particle (TP), modified TP (with unstable wave growth and nonlinear wave evolution), and quasi-linear (QL; with self-consistent time-dependent wave-particle interactions).

(A color version of this figure is available in the online journal.)

Depending on the functions $\Pi(p)$ and $D_{\text{ISM}}(p)$, the resulting CR spectrum generally develops a spectral break for the fixed values of z and t such that $z^2/t \sim D_{\text{NL}}(p) \sim D_{\text{ISM}} \exp(-\Pi)$.

5. DISCUSSION AND OUTLOOK

The CR escape from both active and fading accelerators (old SNRs) is being actively studied through direct observations of CR-illuminated MCs (Aharonian et al. 2008; Abdo et al. 2010a; Giuliani et al. 2011; Aleksić et al. 2012; Uchiyama et al. 2012; Ackermann et al. 2013). To date, most of the information is obtained from the old remnants and they consistently show a broad spectrum of CR escape. This is clearly at odds with an intuitive high-energy-biased escape, seemingly justified by the higher mobility of energetic CRs. Indeed, as CR diffusion coefficient grows with momentum, the TP solution predicts a low-energy cutoff to be present due to the factor $\exp[-z^2/4D_{\text{ISM}}(p)t]$ in the CR distribution at a certain distance z from the source. In a combination with a steep power law or a favorably placed upper cutoff, the escape flux narrowly accumulates toward the maximum energy. The momentum-dependent CR mobility underlies most of the current CR escape models (e.g., Ptuskin & Zirakashvili 2005; Zirakashvili & Ptuskin 2008; Gabici et al. 2009).

Although the same exponential factor is present in the QL solution obtained in this paper, it pertains only to the farthest zone, where the CR partial pressure is much lower (by factor $\Pi^{-1} \ll 1$) than the TP prediction for the same distance from the source and time elapsed from the CR release. Closer to the accelerator, in an extended scale-invariant zone where the CR level is much higher and decays as $1/z$, the escape mechanism is different from the one controlled by the mere energy dependence of the CR diffusivity. It is self-regulated in such a way that, if particles leak excessively in some energy range, they also drive stronger resonant waves to reduce their leakage and vice versa. As a result, the overall escape spectrum relaxes roughly to an equipartition of the CR partial pressure in momentum, e.g., $f_{\text{CR}} \propto p^{-4}$ (with important

deviations described in Section 3.4), which also balances the driver (gradient of CR partial pressure) with the generated waves. No low-energy leakage suppression therefore occurs. The fundamental difference of this leakage mechanism from the TP one is that it is entirely controlled by self-generated rather than prescribed waves, or by waves derived from other energy sources, such as ambient MHD cascades. That is why it predicts energetically much broader leakage than many other approaches do (e.g., Ptuskin & Zirakashvili 2005; Ellison & Bykov 2011).

It should be admitted that the self-confinement solution obtained in this paper is strictly valid for a stopped accelerator, so that there is no CR energy growth and strong plasma flows, such as those found near shocks. Therefore, care should be exercised in comparing this solution with the standard DSA predictions. At the same time, even if CRs were escaping from the DSA through an FEB or an upper momentum cutoff, they would propagate further out diffusively. Yet their escape is often enforced by imposing an ad hoc sudden jump in the diffusion coefficient $D(p, z)$ at a specific momentum p (or FEB position z). Despite this jump, the CR phase space density must be continuous,¹⁰ and for strong CR sources still high enough to drive waves while the CRs escape. From this point on, the solution obtained in this paper may be applied and compared with the DSA predictions, as the waves are driven locally both in momentum and in coordinate space. The only relevant requirement is that particles do not interact with the shock, as implied in most escape models in the first place. But, the feedback from the self-generated waves on the CR escape is not included in the models that predict a peaked energy escape.

Furthermore, the self-regulated escape solution shows a gradual increase of the CR diffusion from a low (Bohm) to

¹⁰ This statement is strictly valid for an FEB imposed by enhanced diffusion in coordinate space. In the case of a jump in momentum (e.g., Ptuskin & Zirakashvili 2005), the situation is more complicated in that the particle distribution should become increasingly anisotropic in pitch angle, as the escape is assumed one sided (upstream). However, an introduction of weak Fermi-II acceleration (diffusion in momentum) would validate this statement also in this case.

high (TP) regime, across the region where $P_{\text{CR}} \propto 1/z$ and the CR diffusion coefficient $D_{\text{CR}} \propto z^2$, thus keeping the flux $-D_{\text{CR}} \nabla \mathcal{P} \approx \text{const}$. Both scalings are clearly inconsistent with a sudden jump in D_{CR} with the corresponding jump in ∇P_{CR} . Moreover, collapsing the scale-invariant region to a point (FEB) would not only change the CR escape flux considerably but also an extended region of enhanced CR pressure would have been lost (see Figure 5). This region (which we loosely dubbed “pedestal” by analogy with the improved confinement regimes in magnetic fusion devices, primarily in tokamaks; e.g., Wagner et al. 1982; Hinton & Staebler 1993; Diamond et al. 1995; Malkov & Diamond 2008; Maggi 2010) may be detectable when it overlaps with MCs. According to the TP theory, the CR density decays as $t^{-d/2}$ in the region of their initial release, with d being the dimensionality of the escape ($d = 1$ for escape along the field). In the self-regulated escape, the CR density stays constant in time in the pedestal region, where $P_{\text{CR}} \propto 1/z$, until this region is overwhelmed by the expanding central plateau where P_{CR} decays as $1/\sqrt{t}$. Before it happens, the CR density is higher than in the TP case (Figure 5), which is a prediction that may soon become testable.

Recent detailed observations of the SNR W44, W51C, IC 443, and W28, surrounded by MC, provide good examples to study possible CR escape scenarios (Aharonian et al. 2008; Abdo et al. 2010a, 2010b, 2010c; Giuliani et al. 2011; Aleksić et al. 2012; Uchiyama et al. 2012). First of all, they almost invariably show spectral breaks that, however, may be understood in terms of the interaction of accelerated protons with a partially ionized dense gas (Malkov et al. 2005, 2011). The indices below and above the breaks are consistent with the following two scenarios. Namely, CR protons may reach the MC while still being accelerated at an SNR shock, or they may escape with a similar spectrum, p^{-4} . As we have shown in the present paper, such escape occurs via the CR interaction with self-generated waves. Another important aspect of these observations regards the morphology of the interaction. Of particular interest is the recent analysis of *Fermi*-LAT results revealing two bright spots of gamma emission adjacent to the central source in W28 (Uchiyama et al. 2012). Their distinct bipolar appearance may be indicative of a CR escape along the local magnetic field.

Note that the anisotropic diffusion of CRs in the form of bipolar CRC may result in quite specific morphologies of extended gamma-ray images—the imprints of CRs interacting with the surrounding diffuse gas are generally concentrated in dense MCs. Since the gamma-ray flux is proportional to the product of densities of CRs and the diffuse gas, we should expect a rather general correlation between the gamma-ray fluxes and the column densities of the interstellar gas. However, it is obvious that in the case of propagation of bipolar CRCs through an inhomogeneous clumpy gaseous environment, the gamma-ray intensity contours can significantly deviate from the CO and 21 cm maps characterizing the spatial distributions of the molecular and atomic gases, respectively. At the same time, the brightest parts of the spatial distribution of gamma rays should correspond to the regions where the CRC overlaps with dense gas clouds *inside the magnetic flux tube* connected with the CR source.

Support by the Department of Energy, grant No. DE-FG02-04ER54738, is gratefully acknowledged. P.H.D. acknowledges support from WCI Program of the National Research Foundation of Korea (NRF; NRF Grant Number WCI 2009-001).

Also, I.V.M. acknowledges support from NASA grants NNX09AC15G and NNX13AC47G.

APPENDIX A

DETAILS OF SELF-SIMILAR SOLUTION

The full expressions for the solution $w(\zeta)$ represented in a short form by Equations (17) and (18) can be written as follows:

$$w = W_0 \begin{cases} e^{\int_0^V dV/\sqrt{R(V)}}, & \zeta \geq \zeta_1 \\ e^{\int_0^{V_1} dV/\sqrt{R(V)} + \int_{V_1}^V dV/\sqrt{R(V)}}, & 0 < \zeta < \zeta_1. \end{cases} \quad (\text{A1})$$

Throughout this Appendix, the positive branch of \sqrt{R} is used. In some cases, it is convenient to represent w in the domain $0 < \zeta < \zeta_1$ as

$$w = w_{\text{max}} e^{-\int_0^V dV/\sqrt{R(V)}}, \quad (\text{A2})$$

where $V_0 \equiv \exp(-q/2)$, i.e., $\zeta(V_0) = 0$, and

$$w_{\text{max}} = W_0 e^{\int_0^{V_1} dV/\sqrt{R(V)} + \int_{V_1}^0 dV/\sqrt{R(V)}}. \quad (\text{A3})$$

For the coordinate ζ we have (Figure 2)

$$\zeta = \sqrt{\frac{2}{w}} \begin{cases} V + 2\sqrt{R(V)} & \zeta \geq \zeta_1 \\ V - 2\sqrt{R(V)} & 0 \leq \zeta < \zeta_1. \end{cases} \quad (\text{A4})$$

The function $w(\zeta)$, implicitly defined by Equations (A1) and (A4), is shown in Figure 3 (see Section 3.2 for approximate explicit results). The partial CR pressure can be represented according to Equation (9) as follows:

$$\mathcal{P}(z, t) = \sqrt{2w(\zeta)/t} V(\zeta) \Big|_{\zeta=z/\sqrt{t}}, \quad z > 1,$$

where $V(\zeta)$ is defined by Equation (A4).

APPENDIX B

HALF-LIFE OF THE CR CLOUD

Equation (25) can be continued as

$$\Pi_1(t_{1/2}) = \frac{1}{2} \Pi = \frac{1}{2} \ln \frac{w_{\text{max}}}{W_0} \equiv \ln \frac{w_{1/2}}{W_0}, \quad (\text{B1})$$

where we have introduced a “half-life” amplitude $w_{1/2}$, which can also be associated with a point $V_{1/2}$ (see Equation (17)),

$$\ln \frac{w_{1/2}}{W_0} = \int_0^{V_{1/2}} dV/\sqrt{R(V)},$$

and with the corresponding self-similar coordinate $\zeta_{1/2} = 1/\sqrt{t_{1/2}}$. In other words, $w_{1/2} = w(\zeta_{1/2}) = w(V_{1/2})$. Note that $w_{1/2}$ can be represented as a geometric mean $w_{1/2} \equiv \sqrt{W_0 w_{\text{max}}}$ (cf. Equation (24)), so that in terms of the function $\ln w(\zeta)$, the point $\zeta_{1/2}$ corresponds to the FWHM. The quantity $V_{1/2}$ can thus be obtained from the following equation:

$$2 \int_0^{V_{1/2}} dV/\sqrt{R(V)} = \int_0^{V_1} dV/\sqrt{R(V)} + \int_{V_0}^{V_1} dV/\sqrt{R(V)}. \quad (\text{B2})$$

In the case of a weak CRC, $\Pi \ll 1$, we obviously have $V_{1/2} < V_0 \sim V_1 \ll 1$. Calculating the integrals in this limit and substituting R from Equation (16), we have

$$\operatorname{erfc}\left(\ln\frac{1}{V_{1/2}} - \frac{q}{2}\right)^{1/2} = \frac{1}{2}$$

or

$$V_{1/2} = e^{-\frac{q}{2} - \sigma} = V_0 e^{-\sigma} \approx V_1 e^{-\sigma} / \left(1 + \frac{1}{2} e^{-q}\right),$$

where $\operatorname{erfc}(\sigma^{1/2}) = 1/2$, so that $\sigma \approx 0.23$. Substituting then $V_{1/2}$ into $\zeta_{1/2}$ from Equation (A4), we obtain the result given by Equation (26).

In the case $\Pi \gg 1$, the integrals on the right-hand side of Equation (B2) are dominated by the upper limit, so the integral on the left-hand side must also be, and we deduce $V_{1/2} \approx V_1$, from which we obtain the nonlinear CR half-life in Equation (28).

REFERENCES

- Abdo, A. A., Ackermann, M., Ajello, M., et al. 2010a, *ApJ*, **718**, 348
 Abdo, A. A., Ackermann, M., Ajello, M., et al. 2010b, *Sci*, **327**, 1103
 Abdo, A. A., Ackermann, M., Ajello, M., et al. 2010c, *ApJ*, **712**, 459
 Achterberg, A. 1981, *A&A*, **98**, 161
 Ackermann, M., Ajello, M., Allafort, A., et al. 2013, *Sci*, **339**, 807
 Aharonian, F., Akhperjanian, A. G., Bazer-Bachi, A. R., et al. 2008, *A&A*, **481**, 401
 Aharonian, F. A., & Atoyan, A. M. 1996, *A&A*, **309**, 917
 Aharonian, F. A., Drury, L. O., & Voelk, H. J. 1994, *A&A*, **285**, 645
 Aleksić, J., Alvarez, E. A., Antonelli, L. A., et al. 2012, *A&A*, **541**, A13
 Bell, A. R. 1978, *MNRAS*, **182**, 147
 Bell, A. R. 2004, *MNRAS*, **353**, 550
 Beresnyak, A., & Lazarian, A. 2008, *ApJ*, **678**, 961
 Berezhko, E. G. 1996, *Aph*, **5**, 367
 Bisnovatyi-Kogan, G. S., & Silich, S. A. 1995, *RvMP*, **67**, 661
 Blasi, P., & Amato, E. 2012, *JCAP*, **12**, 010
 Brunetti, M. T., & Codino, A. 2000, *ApJ*, **528**, 789
 Burgess, D., Möbius, E., & Scholer, M. 2012, *SSRv*, **50**
 Bykov, A. M., Osipov, S. M., & Toptygin, I. N. 2009, *AstL*, **35**, 555
 Diamond, P. H., Lebedev, V. B., Newman, D. E., & Carreras, B. A. 1995, *PhPl*, **2**, 3685
 Drury, L. O. 1983, *RPPH*, **46**, 973
 Drury, L. O. 2011, *MNRAS*, **415**, 1807
 Drury, L. O., Duffy, P., Eichler, D., & Mastichiadis, A. 1999, *A&A*, **347**, 370
 Drury, L. O., Ellison, D. E., Aharonian, F. A., et al. 2001, *SSRv*, **99**, 329
 Drury, L. O. C., & Falle, S. A. E. G. 1986, *MNRAS*, **223**, 353
 Ellison, D. C., & Bykov, A. M. 2011, *ApJ*, **731**, 87
 Farmer, A. J., & Goldreich, P. 2004, *ApJ*, **604**, 671
 Fujita, Y., Takahara, F., Ohira, Y., & Iwasaki, K. 2011, *MNRAS*, **415**, 3434
 Funk, S. 2012, arXiv:1204.4529
 Gabici, S. 2011, *MmSAI*, **82**, 760
 Gabici, S., Aharonian, F. A., & Casanova, S. 2009, *MNRAS*, **396**, 1629
 Galinsky, V. L., & Shevchenko, V. I. 2007, *ApJL*, **669**, L109
 Galinsky, V. L., & Shevchenko, V. I. 2011, *ApJ*, **734**, 106
 Gargaté, L., & Spitkovsky, A. 2012, *ApJ*, **744**, 67
 Giuliani, A., Cardillo, M., Tavani, M., et al. 2011, *ApJL*, **742**, L30
 Goldreich, P., & Sridhar, S. 1997, *ApJ*, **485**, 680
 Gull, S. F. 1973, *MNRAS*, **161**, 47
 Hinton, F. L., & Staebler, G. M. 1993, *PhFIB*, **5**, 1281
 Inoue, T., Yamazaki, R., Inutsuka, S.-i., & Fukui, Y. 2012, *ApJ*, **744**, 71
 Ivanov, A. A., Rusanov, V. D., & Sagdeev, R. Z. 1970, *JETPL*, **12**, 20
 Kang, H., Ryu, D., & Jones, T. W. 2009, *ApJ*, **695**, 1273
 Kirk, J. G., & Dendy, R. O. 2001, *JPhG*, **27**, 1589
 Lagage, P. O., & Cesarsky, C. J. 1983, *A&A*, **125**, 249
 Maggi, C. F. 2010, *NucFu*, **50**, 066001
 Malkov, M. A., & Diamond, P. H. 2006, *ApJ*, **642**, 244
 Malkov, M. A., & Diamond, P. H. 2008, *PhPl*, **15**, 122301
 Malkov, M. A., Diamond, P. H., & Jones, T. W. 2002, *ApJ*, **571**, 856
 Malkov, M. A., Diamond, P. H., & Sagdeev, R. Z. 2005, *ApJL*, **624**, L37
 Malkov, M. A., Diamond, P. H., & Sagdeev, R. Z. 2010, *PPCF*, **52**, 124006
 Malkov, M. A., Diamond, P. H., & Sagdeev, R. Z. 2011, *NatCo*, **2**/1195
 Malkov, M. A., & Völk, H. J. 1995, *A&A*, **300**, 605
 Moskalenko, I. V., Porter, T. A., Malkov, M. A., & Diamond, P. H. 2007, arXiv:0705.3854
 Ohira, Y., Murase, K., & Yamazaki, R. 2011, *MNRAS*, **410**, 1577
 Ptuskin, V. S., & Zirakashvili, V. N. 2005, *A&A*, **429**, 755
 Ptuskin, V. S., Zirakashvili, V. N., & Plesser, A. A. 2008, *AdSR*, **42**, 486
 Reville, B., Kirk, J. G., & Duffy, P. 2009, *ApJ*, **694**, 951
 Reynoso, E. M., Hughes, J. P., & Moffett, D. A. 2013, *AJ*, **145**, 104
 Rosner, R., & Bodo, G. 1996, *ApJL*, **470**, L49
 Ryutov, D. D., & Sagdeev, R. Z. 1970, *JETP*, **31**, 396
 Skilling, J. 1975, *MNRAS*, **172**, 557
 Strong, A. W., Moskalenko, I. V., & Ptuskin, V. S. 2007, *ARNPS*, **57**, 285
 Tavani, M., Giuliani, A., Chen, A. W., et al. 2010, *ApJL*, **710**, L151
 Torres, D. F., Li, H., Chen, Y., et al. 2011, *MNRAS*, **417**, 3072
 Truelove, J. K., & McKee, C. F. 1999, *ApJS*, **120**, 299
 Uchiyama, Y., Funk, S., Katagiri, H., et al. 2012, *ApJL*, **749**, L35
 Völk, H. J., Berezhko, E. G., & Ksenofontov, L. T. 2003, *A&A*, **409**, 563
 Wagner, F., Becker, G., Behringer, K., et al. 1982, *PhRvL*, **49**, 1408
 Wentzel, D. G. 1974, *ARA&A*, **12**, 71
 Yan, H., Lazarian, A., & Schlickeiser, R. 2012, *ApJ*, **745**, 140
 Zirakashvili, V. N., & Ptuskin, V. S. 2008, *ApJ*, **678**, 939